Synchronised trajectory-tracking control of multiple 3-DOF experimental helicopters

J. Shan, H.-T. Liu and S. Nowotny

Abstract: A synchronised trajectory-tracking control strategy is proposed for multiple experimental three-degrees-of-freedom helicopters. The model-based controller includes a feedforward compensation term and a PD feedback control term. Asymptotic convergence is achieved for both trajectory tracking and motion synchronisation. A proposed generalised synchronisation error concept allows the design of different synchronisation strategies so that different synchronisation performance can be reached. Experimental results verify the effectiveness of the proposed controller.

1 Introduction

With the development in technology and the requirement for high efficiency and productivity there is tremendous demand for multicomponent systems, such as applications in manufacturing industry, aerospace operations and so on. Such multicomponent systems often work under co-operative or co-ordinated schemes. According to [1], synchronisation may be defined as the mutual time conformity of two or more processes. Co-operation, co-ordination and synchronisation are intimately linked subjects and usually they are used as synonyms to describe the same kind of behaviour [2].

For mechanical systems, motion synchronisation is of great importance as soon as two or more systems have to co-operate. The co-operative behaviour gives flexibility and maneuverability that cannot be achieved by an individual system [3]. Motion synchronisation has received a lot of attention in recent years. The cross-coupling concept is first proposed in [4] to address the motion synchronisation problem. It is combined with an adaptive feedforward controller to achieve speed synchronisation of two motion axes [5], as well as position and speed synchronisation of two gyro motions [6]. The position synchronisation of multiple robot systems with only position measurements is studied in [2], where coupling errors are introduced to create interconnections that render mutual synchronisation of the robots. This method is also applied to the synchronisation control of multiple mobile robots [3]. For multiple spacecraft formation flying, a synchronised rotation strategy has been studied in [7]. A clock control strategy is used to synchronise the motion of a pair of independent windshield wipers by delaying the reference trajectory of the follower wiper when the leader is behind its reference trajectory [8].

IEE Proceedings online no. 20050008

doi: 10.1049/ip-cta:20050008

Paper first received 10th January and in revised form 14th April 2005

J. Shan and H.-T. Liu are with the Institute for Aerospace Studies, University of Toronto, 4925 Dufferin St., Toronto, Canada M3H 5T6

S. Nowotny is with the Faculty of Aerospace Engineering and Geodesy, University of Stuttgart, Pfaffenwaldring 27, D-70569 Stuttgart, Germany

E-mail: shan@utias.utoronto.ca

This paper presents a synchronised trajectory-tracking control of multiple three-degrees-of-freedom (3-DOF) helicopters. The proposed controller includes a feedforward dynamic term and a PD feedback term. Both the attitude trajectory tracking errors of all involved 3-DOF helicopters and the attitude synchronisation errors among them will achieve asymptotic convergence simultaneously. The transient attitude synchronisation behaviour is further improved by using a generalised synchronisation error strategy. Experiments of multiple 3-DOF helicopters in laboratory are conducted to verify the proposed controller.

2 Modelling of 3-DOF helicopter

Many experimental facilities have been developed in single/multiple rotorcraft/helicopter research [9–13]. The Flight Systems and Control (FSC) Laboratory of the University of Toronto facilitates several Quanser's 3-DOF helicopters (http://www.quanser.com) for study on multi-vehicle co-ordination/co-operative control, multivehicle formation flight/flying control, and advanced controller development. Figure 1 shows a photograph of helicopter equipped with active disturbance systems (ADS), which can emulate uncertainties in system parameters and act as disturbances to the control system. Figure 2 gives the detailed schematic diagram of the acting forces on the system. Based on this diagram, the equations for three DOFs, elevation, pitch, and travel of a helicopter can be obtained as follows.

- *Elevation axis*: The elevation motion can be described by the following differential equation:

$$\begin{aligned} J_e\ddot{\alpha} &= K_f l_a \cos(\beta)(V_f + V_b) - mgl_a \sin(\alpha + \alpha_0) \\ &= K_f l_a \cos(\beta) V_s - mgl_a \sin(\alpha + \alpha_0) \end{aligned} \quad (1)$$

where α is the elevation angle, α_0 is the angle between helicopter arm and its base, β is the pitch angle, J_e is the moment of inertia of the system about the elevation axis, K_f is the force constant of the motor/propeller combination, l_a is the distance from the pivot point to the helicopter body, V_f and V_b are the respective voltages applied to the front and back motors, V_s is the sum of V_f and V_b, m is the effective mass about the elevation axis, g is the gravity constant. For 3-DOF helicopter with ADS, the effective mass m is adjustable.

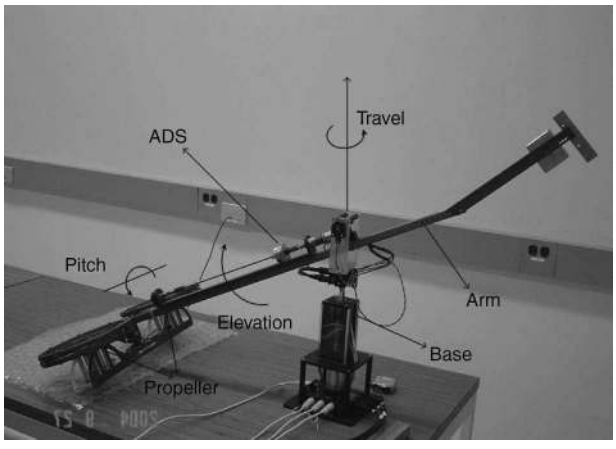

Fig. 1 *Photograph of 3-DOF helicopter with ADS*

• *Pitch axis:* The pitch axis is controlled by the difference of the forces generated by the propellers

$$J_p\ddot{\beta} = K_f l_h(V_f - V_b) = K_f l_h V_d \tag{2}$$

where J_p is the moment of inertia of the system about the pitch axis, l_h is the distance from the pitch axis to either motor, V_d is the difference between the voltage applied to the front and back motors. If the force generated by the front motor is higher than the force generated by the back motor, the helicopter body will pitch up (positive). The pitch angle is limited to within $(-\pi/2, \pi/2)$ mechanically during experiment.

• *Travel axis:* The only way to apply a force in the travel direction is to pitch body of the helicopter. The corresponding dynamic equation of travel axis is:

$$\begin{aligned} J_t\ddot{\gamma} &= K_f l_a \sin\beta \sin(\alpha+\alpha_0)(V_f + V_b) \\ &\quad + K_f l_h \cos(\alpha+\alpha_0)(V_f - V_b) \\ &= K_f l_a \sin\beta \sin(\alpha+\alpha_0)V_s + K_f l_h \cos(\alpha+\alpha_0)V_d \end{aligned} \tag{3}$$

where γ is the travel angle, J_t is the moment of inertia about the travel axis. Moreover, if $(\alpha+\alpha_0) = \pi/2$, i.e. the arm is in horizontal position, the travel motion becomes

$$J_t\ddot{\gamma} = K_f l_a \sin\beta \sin(\alpha+\alpha_0)V_s \tag{4}$$

which can be verified easily from Fig. 2.
From this modelling we know that the elevation acceleration is a function of the sum of the voltages applied to the two motors, and the pitch acceleration is a function of difference between them. If the pitch angle β and elevation angle α are constants and β is a small value, the travel motion become

$$J_t\ddot{\gamma} = K\beta \tag{5}$$

where $K = K_f l_a V_s \sin(\alpha+\alpha_0)$ and this equation means that the travel acceleration is governed by the pitch angle. Considering these modelling characteristics and assuming the travel motion can be achieved by high-precise pitch tracking, we can simplify the 3-DOF attitude dynamics to a 2-DOF one, which includes elevation and pitch motion, as given in (6)

$$\begin{bmatrix} \frac{J_e}{K_f l_a \cos\beta} & 0 \\ 0 & \frac{J_p}{K_f l_h} \end{bmatrix} \begin{bmatrix} \ddot{\alpha} \\ \ddot{\beta} \end{bmatrix} + \begin{bmatrix} \frac{mg\sin(\alpha+\alpha_0)}{K_f\cos\beta} \\ 0 \end{bmatrix} = \begin{bmatrix} V_s \\ V_d \end{bmatrix} \tag{6}$$

and in matrix format

$$\boldsymbol{J}\ddot{\boldsymbol{\Theta}} + \boldsymbol{N}(\Theta, m, K_f) = \boldsymbol{v} \tag{7}$$

where $\boldsymbol{J} \in \mathbb{R}^{2\times 2} = \mathrm{diag}\left[J_e/K_f l_a \cos\beta \quad J_p/K_f l_h\right]$ is the moment of inertia, $\boldsymbol{\Theta} \in \mathbb{R}^2 = [\alpha \quad \beta]^T$ is the attitude (elevation and pitch) vector, $\boldsymbol{N}(\Theta, m, K_f) \in \mathbb{R}^2 = \left[mg\sin(\alpha+\alpha_0)/K_f\cos\beta \quad 0\right]^T$ is the nonlinear term, and $\boldsymbol{v} \in \mathbb{R}^2 = [V_s \quad V_d]^T$ is control voltage vector. For $-\pi/2 < \beta < \pi/2$, the inertia matrix $\boldsymbol{J}$ is a positive-definite matrix.

Consider n such helicopters, we have a set of dynamic equations

$$\begin{aligned} \boldsymbol{J}_1\ddot{\boldsymbol{\Theta}}_1 + \boldsymbol{N}_1(\Theta_1, m_1, K_{f1}) &= \boldsymbol{v}_1 \\ \boldsymbol{J}_2\ddot{\boldsymbol{\Theta}}_2 + \boldsymbol{N}_2(\Theta_2, m_2, K_{f2}) &= \boldsymbol{v}_2 \\ &\vdots \\ \boldsymbol{J}_i\ddot{\boldsymbol{\Theta}}_i + \boldsymbol{N}_i(\Theta_i, m_i, K_{fi}) &= \boldsymbol{v}_i \\ &\vdots \\ \boldsymbol{J}_n\ddot{\boldsymbol{\Theta}}_n + \boldsymbol{N}_n(\Theta_n, m_n, K_{fn}) &= \boldsymbol{v}_n \end{aligned} \tag{8}$$

and in matrix format as

$$\boldsymbol{I}\ddot{\tilde{\boldsymbol{\Theta}}} + \tilde{\boldsymbol{N}}(\Theta, \boldsymbol{m}, \boldsymbol{K}_f) = \boldsymbol{V} \tag{9}$$

where $\boldsymbol{J}_i, \Theta_i, \boldsymbol{N}_i(\cdot)$ and $\boldsymbol{v}_i$ have the same expressions as $\boldsymbol{J}, \Theta, \boldsymbol{N}(\cdot)$ and $\boldsymbol{v}$, subscript i denotes the ith 3-DOF helicopter, $\tilde{\boldsymbol{\Theta}} \in \mathbb{R}^{2n}$, $\tilde{\boldsymbol{N}} \in \mathbb{R}^{2n}$, $\boldsymbol{V} \in \mathbb{R}^{2n}$, $\boldsymbol{m} \in \mathbb{R}^n$, $\boldsymbol{K}_f \in \mathbb{R}^n$, are vectors, $\boldsymbol{I} \in \mathbb{R}^{2n\times 2n}$ is a diagonal inertia matrix, and they have the following expressions:

$$\begin{aligned} \boldsymbol{I} &= \mathrm{diag}[\boldsymbol{J}_1 \quad \boldsymbol{J}_2 \quad \cdots \quad \boldsymbol{J}_i \quad \cdots \quad \boldsymbol{J}_n] \\ \tilde{\boldsymbol{\Theta}} &= [\boldsymbol{\Theta}_1^T \quad \boldsymbol{\Theta}_2^T \quad \cdots \quad \boldsymbol{\Theta}_i^T \quad \cdots \quad \boldsymbol{\Theta}_n^T]^T \\ &= [\alpha_1 \quad \beta_1 \quad \alpha_2 \quad \beta_2 \quad \cdots \quad \alpha_i \quad \beta_i \quad \cdots \quad \alpha_n \quad \beta_n]^T \\ \boldsymbol{m} &= [m_1 \quad m_2 \quad \cdots \quad m_i \quad \cdots \quad m_n]^T \\ \boldsymbol{K}_f &= [K_{f1} \quad K_{f2} \quad \cdots \quad K_{fi} \quad \cdots \quad K_{fn}]^T \\ \tilde{\boldsymbol{N}} &= [\boldsymbol{N}_1^T \quad \boldsymbol{N}_2^T \quad \cdots \quad \boldsymbol{N}_i^T \quad \cdots \quad \boldsymbol{N}_n^T]^T \\ \boldsymbol{V} &= [\boldsymbol{v}_1^T \quad \boldsymbol{v}_2^T \quad \cdots \quad \boldsymbol{v}_i^T \quad \cdots \quad \boldsymbol{v}_n^T]^T \\ &= [V_{s1} \quad V_{d1} \quad V_{s2} \quad V_{d2} \quad \cdots \quad V_{si} \quad V_{di} \quad \cdots \quad V_{sn} \quad V_{dn}]^T \end{aligned}$$

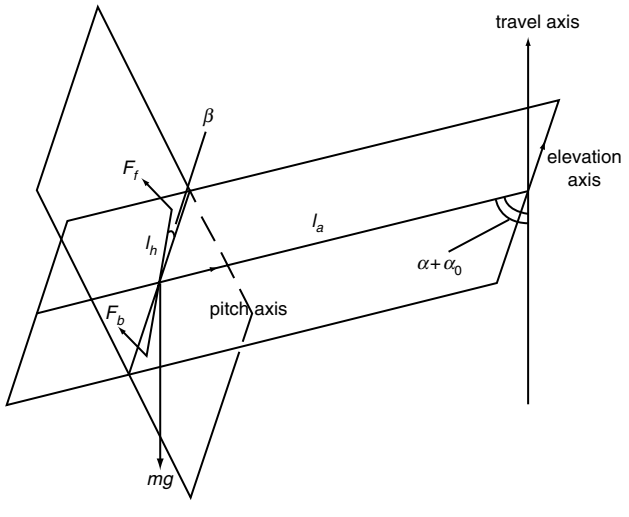

Fig. 2 *Schematic diagram of acting forces*

3 Synchronisation controller design

3.1 Control objective

First we define $\boldsymbol{E}(t) \in \mathbb{R}^{2n}, \dot{\boldsymbol{E}}(t) \in \mathbb{R}^{2n}$ as the attitude angle and attitude angular velocity tracking error vectors of

n 3-DOF helicopters. $\boldsymbol{\Xi}(t) \in \mathbb{R}^{2n}$ and $\dot{\boldsymbol{\Xi}}(t)$ are defined as the synchronisation error and the error derivative vectors, respectively. They then have the following expressions:

$$\boldsymbol{E}(t) \triangleq [\, e_1^T(t) \quad e_2^T(t) \quad \cdots \quad e_i^T(t) \quad \cdots \quad e_n^T(t) \,]^T \tag{10}$$

$$\dot{\boldsymbol{E}}(t) \triangleq [\, \dot{e}_1^T(t) \quad \dot{e}_2^T(t) \quad \cdots \quad \dot{e}_i^T(t) \quad \cdots \quad \dot{e}_n^T(t) \,]^T \tag{11}$$

$$\boldsymbol{\Xi}(t) \triangleq [\, \varepsilon_1^T(t) \quad \varepsilon_2^T(t) \quad \cdots \quad \varepsilon_i^T(t) \quad \cdots \quad \varepsilon_n^T(t) \,]^T \tag{12}$$

$$\dot{\boldsymbol{\Xi}}(t) \triangleq [\, \dot{\varepsilon}_1^T(t) \quad \dot{\varepsilon}_2^T(t) \quad \cdots \quad \dot{\varepsilon}_i^T(t) \quad \cdots \quad \dot{\varepsilon}_n^T(t) \,]^T \tag{13}$$

$$\boldsymbol{e}_i(t) \triangleq \Theta_d(t) - \Theta_i(t) \tag{14}$$

$$\dot{\boldsymbol{e}}_i(t) \triangleq \dot{\Theta}_d(t) - \dot{\Theta}_i(t) \tag{15}$$

where $\Theta_d \in \mathbb{R}^2$ and $\dot{\Theta}_d \in \mathbb{R}^2$ are the desired trajectories for attitude angles and angular velocities of all 3-DOF helicopters. The definition of the synchronisation error is given in the subsequent Section.

To track the trajectory synchronously for multiple 3-DOF helicopters, one must satisfy the following three criteria. First, the designed controller should guarantee the stability of the attitude trajectory tracking errors of all involved systems. Secondly, the controller should also guarantee the stability of the synchronisation errors. Thirdly, the controller should regulate the attitude motion to track the desired trajectory at the same rate so that the synchronisation errors go to zero simultaneously.

In short, the control objective becomes $\boldsymbol{E}(t) \to 0, \boldsymbol{\Xi}(t) \to 0$ as $t \to \infty$.

3.2 Generalised synchronisation error

Synchronisation error is introduced to identify the performance of synchronisation controller, i.e. how the trajectory of each 3-DOF helicopter converges with respect to each other. There are various ways to choose the synchronisation error. For example, in [2] the authors include the error information of all systems into the synchronisation error of each system. However, when there is a large number of involved systems, this synchronisation strategy will lead to intensive online computational work. In this paper we propose a more feasible and efficient synchronisation error $\boldsymbol{\Xi}(t)$, which is a linear combination of attitude tracking error $\boldsymbol{E}(t)$.

$$\boldsymbol{\Xi}(t) = \boldsymbol{T}\boldsymbol{E}(t) \tag{16}$$

where $\boldsymbol{T} \in \mathbb{R}^{2n \times 2n}$ is a generalised synchronisation transformation matrix. By choosing a different matrix $\boldsymbol{T}$ we can form different synchronisation errors. For example, if we choose the following synchronisation transformation matrix $\boldsymbol{T}$

$$\boldsymbol{T} = \begin{bmatrix} \mathrm{I} & -\mathrm{I} & & & \\ & \mathrm{I} & -\mathrm{I} & & \\ & & \ddots & \ddots & \\ & & & \mathrm{I} & -\mathrm{I} \\ -\mathrm{I} & & & & \mathrm{I} \end{bmatrix} \tag{17}$$

we will get the following synchronisation error formula:

$$\begin{aligned} \varepsilon_1(t) &= \boldsymbol{e}_1(t) - \boldsymbol{e}_2(t) \\ \varepsilon_2(t) &= \boldsymbol{e}_2(t) - \boldsymbol{e}_3(t) \\ \varepsilon_3(t) &= \boldsymbol{e}_3(t) - \boldsymbol{e}_4(t) \\ &\vdots \\ \varepsilon_n(t) &= \boldsymbol{e}_n(t) - \boldsymbol{e}_1(t) \end{aligned} \tag{18}$$

The synchronisation error in (18) has been used in [14] for the synchronisation control of multiple robotic manipulators.

Another more complicated synchronisation error formula in (19) can be obtained by applying the synchronisation transformation matrix $\boldsymbol{T}$ given in (20)

$$\begin{aligned} \varepsilon_1(t) &= 2\boldsymbol{e}_1(t) - \boldsymbol{e}_2(t) - \boldsymbol{e}_n(t) \\ \varepsilon_2(t) &= 2\boldsymbol{e}_2(t) - \boldsymbol{e}_3(t) - \boldsymbol{e}_1(t) \\ \varepsilon_3(t) &= 2\boldsymbol{e}_3(t) - \boldsymbol{e}_4(t) - \boldsymbol{e}_2(t) \\ &\vdots \\ \varepsilon_n(t) &= 2\boldsymbol{e}_n(t) - \boldsymbol{e}_n(t) - \boldsymbol{e}_{n-1}(t) \end{aligned} \tag{19}$$

$$\boldsymbol{T} = \begin{bmatrix} 2I & -I & & & -I \\ -I & 2I & -I & & \\ & \ddots & \ddots & \ddots & \\ & & -I & 2I & -I \\ -I & & & -I & 2I \end{bmatrix} \tag{20}$$

In (18, 19) each individual helicopter's synchronisation error is a linear combination of its tracking error and one or two adjoining helicopters' tracking errors. With more tracking errors involved one may expect to achieve better performance. However, it is compromised by the computational challenge. In this paper the synchronisation errors in (18, 19) are applied for our investigation.

3.3 Coupled attitude error

For controller design a coupled attitude error $\boldsymbol{E}^*(t) \in \mathbb{R}^{2n}$ that contains both the attitude trajectory tracking error $\boldsymbol{E}(t)$ and the synchronisation error $\boldsymbol{\Xi}(t)$ is further introduced

$$\boldsymbol{E}^*(t) = \boldsymbol{E}(t) + \boldsymbol{B}\boldsymbol{T}^T \int_0^t \boldsymbol{\Xi} d\tau \tag{21}$$

where $\boldsymbol{E}^* \triangleq [\boldsymbol{e}_1^{*T}\, \boldsymbol{e}_2^{*T} \cdots \boldsymbol{e}_n^{*T}]^T, \boldsymbol{B} \in \mathbb{R}^{2n \times 2n} \triangleq \mathrm{diag}[\underline{\boldsymbol{B}}\, \underline{\boldsymbol{B}} \cdots \underline{\boldsymbol{B}}]$ is a positive-definite coupling gain matrix and $\underline{\boldsymbol{B}} \in \mathbb{R}^{2\times 2}$ is also diagonal matrix.

Correspondingly the coupled angular velocity error can be expressed as

$$\dot{\boldsymbol{E}}^*(t) = \dot{\boldsymbol{E}}(t) + \boldsymbol{B}\boldsymbol{T}^T \boldsymbol{\Xi}(t) \tag{22}$$

For the synchronisation transformation matrix $\boldsymbol{T}$ in (17), the coupled attitude errors become

$$\begin{aligned} \boldsymbol{e}_1^*(t) &= \boldsymbol{e}_1(t) + \underline{\boldsymbol{B}} \int_0^t (\varepsilon_1(\tau) - \varepsilon_n(\tau)) d\tau \\ \boldsymbol{e}_2^*(t) &= \boldsymbol{e}_2(t) + \underline{\boldsymbol{B}} \int_0^t (\varepsilon_2(\tau) - \varepsilon_1(\tau)) d\tau \\ \boldsymbol{e}_3^*(t) &= \boldsymbol{e}_3(t) + \underline{\boldsymbol{B}} \int_0^t (\varepsilon_3(\tau) - \varepsilon_2(\tau)) d\tau \\ &\vdots \\ \boldsymbol{e}_n^*(t) &= \boldsymbol{e}_n(t) + \underline{\boldsymbol{B}} \int_0^t (\varepsilon_n(\tau) - \varepsilon_{n-1}(\tau)) d\tau \end{aligned} \tag{23}$$

Similarly the coupled attitude errors corresponding to $\boldsymbol{T}$ in (20) are

$$\begin{aligned}
\boldsymbol{e}_1^*(t) &= \boldsymbol{e}_1(t) + \underline{\boldsymbol{B}} \int_0^t (2\varepsilon_1(\tau) - \varepsilon_2(\tau) - \varepsilon_n(\tau))d\tau \\
\boldsymbol{e}_2^*(t) &= \boldsymbol{e}_2(t) + \underline{\boldsymbol{B}} \int_0^t (2\varepsilon_2(\tau) - \varepsilon_3(\tau) - \varepsilon_1(\tau))d\tau \\
\boldsymbol{e}_3^*(t) &= \boldsymbol{e}_3(t) + \underline{\boldsymbol{B}} \int_0^t (2\varepsilon_3(\tau) - \varepsilon_4(\tau) - \varepsilon_2(\tau))d\tau \\
&\vdots \\
\boldsymbol{e}_n^*(t) &= \boldsymbol{e}_n(t) + \underline{\boldsymbol{B}} \int_0^t (2\varepsilon_n(\tau) - \varepsilon_n(\tau) - \varepsilon_{n-1}(\tau))d\tau
\end{aligned} \tag{24}$$

From (23) we see that the synchronisation error $\varepsilon_i(t)$ appears in $\boldsymbol{e}_i^*(t)$ and $\boldsymbol{e}_{i+1}^*(t)$ with opposite sign. Similar observation is obtained for the synchronisation error in (24). In this way, the coupled attitude errors are driven in opposite directions by $\varepsilon_i(t)$, which contributes to the elimination of the synchronisation error $\varepsilon_i(t)$.

3.4 Synchronised trajectory tracking controller

The synchronised trajectory tracking controller includes two parts: feedback and feedforward. The feedback part employs PD control law plus synchronisation feedback term

$$\boldsymbol{u}(t) = \boldsymbol{K}_P\boldsymbol{E}^*(t) + \boldsymbol{K}_D\dot{\boldsymbol{E}}^*(t) + \boldsymbol{K}_s\boldsymbol{T}^T\boldsymbol{\Xi}(t) \tag{25}$$

where $\boldsymbol{K}_P, \boldsymbol{K}_D, \boldsymbol{K}_s \in \mathbb{R}^{2n\times 2n}$ are constant, diagonal, positive-definite, control gain matrices. By defining the following coupled tracking error

$$\boldsymbol{r}(t) = \dot{\boldsymbol{E}}^*(t) + \boldsymbol{\Lambda}\boldsymbol{E}^*(t) \tag{26}$$

we can rewrite (25) as

$$\boldsymbol{u}(t) = \boldsymbol{K}\boldsymbol{r}(t) + \boldsymbol{K}_s\boldsymbol{T}^T\boldsymbol{\Xi}(t) \tag{27}$$

where $\boldsymbol{r}(t) \triangleq [\boldsymbol{r}_1^T(t) \quad \boldsymbol{r}_2^T(t) \quad \cdots \quad \boldsymbol{r}_n^T(t)]^T$, $\boldsymbol{\Lambda} \in \mathbb{R}^{2n\times 2n} \triangleq \text{diag}[\boldsymbol{\Lambda}_1 \quad \boldsymbol{\Lambda}_2 \quad \cdots \quad \boldsymbol{\Lambda}_n]$ and its element $\boldsymbol{\Lambda}_{ikl} = K_{Pi_{kl}}/K_{Di_{kl}}$, $\boldsymbol{K} = \boldsymbol{K}_D$. The feedforward part $\tilde{\boldsymbol{u}}(t)$ is designed to be

$$\tilde{\boldsymbol{u}}(t) = \boldsymbol{I}\boldsymbol{\Phi} + \tilde{\boldsymbol{N}}(\boldsymbol{\Theta}, \boldsymbol{m}, \boldsymbol{K}_f) \tag{28}$$

with $\boldsymbol{\Phi} = \ddot{\boldsymbol{\Theta}}_d + \boldsymbol{\Lambda}\dot{\boldsymbol{E}}^* + \boldsymbol{B}\boldsymbol{T}^T\dot{\boldsymbol{\Xi}}$. Therefore the total control voltage $\boldsymbol{V}(t)$ is

$$\begin{aligned}
\boldsymbol{V}(t) &= \tilde{\boldsymbol{u}}(t) + \boldsymbol{u}(t) \\
&= \boldsymbol{I}\boldsymbol{\Phi} + \tilde{\boldsymbol{N}}(\boldsymbol{\Theta}, \boldsymbol{m}, \boldsymbol{K}_f) + \boldsymbol{K}\boldsymbol{r}(t) + \boldsymbol{K}_s\boldsymbol{T}^T\boldsymbol{\Xi}(t)
\end{aligned} \tag{29}$$

Figure 3 gives the overall structure of the proposed synchronisation controller.

Theorem 1: The proposed synchronisation controller in (27, 28, 29) guarantees asymptotic convergence to zero of both attitude trajectory tracking error $\boldsymbol{E}(t)$ and synchronisation error $\boldsymbol{\Xi}(t)$ for pitch angle $\beta \in (-\pi/2, \pi/2)$, i.e.

$$\lim_{t\to\infty} \boldsymbol{E}(t),\ \boldsymbol{\Xi}(t) = 0 \tag{30}$$

Proof: Choose the following Lyapunov function

$$\begin{aligned}
V(\boldsymbol{r}, \tilde{\boldsymbol{\Psi}}, \boldsymbol{\Xi}) \triangleq\ & \frac{1}{2}\boldsymbol{r}^T\boldsymbol{I}\boldsymbol{r} + \frac{1}{2}\tilde{\boldsymbol{\Psi}}^T\boldsymbol{\Gamma}^{-1}\tilde{\boldsymbol{\Psi}} + \frac{1}{2}\boldsymbol{\Xi}^T\boldsymbol{K}_s\boldsymbol{\Xi} \\
& + \frac{1}{2}\left(\int \boldsymbol{T}^T\boldsymbol{\Xi}d\tau\right)^T\boldsymbol{B}\boldsymbol{\Lambda}\boldsymbol{K}_s\left(\int \boldsymbol{T}^T\boldsymbol{\Xi}d\tau\right)
\end{aligned} \tag{31}$$

Because $\boldsymbol{\Gamma}^{-1}, \boldsymbol{K}_s, \boldsymbol{B}\boldsymbol{\Lambda}$ are all positive-definite matrices and $\boldsymbol{I}$ is positive-definite when pitch angle $\beta \in (-\pi/2, \pi/2)$, thus the Lyapunov function $V(\boldsymbol{r}, \boldsymbol{\Xi})$ is a positive-definite function when $\beta \in (-\pi/2, \pi/2)$. Differentiating (31) with respect to time t yields

$$\begin{aligned}
\dot{V}(\boldsymbol{r}, \boldsymbol{\Xi}) =\ & \boldsymbol{r}^T\boldsymbol{I}\dot{\boldsymbol{r}} + \boldsymbol{\Xi}^T\boldsymbol{K}_s\dot{\boldsymbol{\Xi}} \\
& + \left(\int \boldsymbol{T}^T\boldsymbol{\Xi}d\tau\right)^T\boldsymbol{B}\boldsymbol{\Lambda}\boldsymbol{K}_s\boldsymbol{T}^T\boldsymbol{\Xi}
\end{aligned} \tag{32}$$

Differentiating (26) with respect to time t and considering (10, 14, 21, 22),

$$\begin{aligned}
\dot{\boldsymbol{r}} &= \ddot{\boldsymbol{E}}^* + \boldsymbol{\Lambda}\dot{\boldsymbol{E}}^* \\
&= \ddot{\boldsymbol{E}} + \boldsymbol{B}\boldsymbol{T}^T\dot{\boldsymbol{\Xi}} + \boldsymbol{\Lambda}\dot{\boldsymbol{E}}^* \\
&= \ddot{\boldsymbol{\Theta}}_d - \ddot{\boldsymbol{\Theta}} + \boldsymbol{B}\boldsymbol{T}^T\dot{\boldsymbol{\Xi}} + \boldsymbol{\Lambda}\dot{\boldsymbol{E}}^* \\
&= \boldsymbol{\Phi} - \ddot{\boldsymbol{\Theta}}
\end{aligned} \tag{33}$$

Multiplying $\boldsymbol{I}$ at both sides of (33) and substituting with (9, 29) obtains

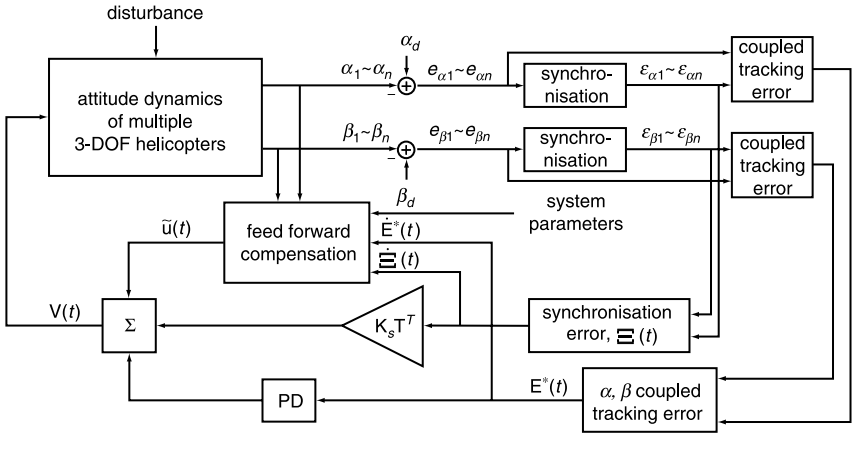

Fig. 3 *Structure of control system*

$$
\begin{aligned}
\boldsymbol{I}\dot{\boldsymbol{r}} &= \boldsymbol{I}\boldsymbol{\Phi} - \boldsymbol{I}\ddot{\boldsymbol{\Theta}} \\
&= \boldsymbol{I}\boldsymbol{\Phi} - (\boldsymbol{V} - \tilde{\boldsymbol{N}}(\boldsymbol{\Theta}, \boldsymbol{m}, \boldsymbol{K}_f)) \\
&= \boldsymbol{I}\boldsymbol{\Phi} + \tilde{\boldsymbol{N}}(\boldsymbol{\Theta}, \boldsymbol{m}, \boldsymbol{K}_f) - (\boldsymbol{I}\boldsymbol{\Phi} + \tilde{\boldsymbol{N}}(\boldsymbol{\Theta}, \boldsymbol{m}, \boldsymbol{K}_f) \\
&\quad + \boldsymbol{K}\boldsymbol{r}(t) + \boldsymbol{K}_s\boldsymbol{T}^T\boldsymbol{\Xi}(t)) \\
&= -\boldsymbol{K}\boldsymbol{r} - \boldsymbol{K}_s\boldsymbol{T}^T\boldsymbol{\Xi}
\end{aligned} \tag{34}
$$

Substituting (34) into (32) yields

$$
\begin{aligned}
\dot{V}(\boldsymbol{r}, \boldsymbol{\Xi}) &= \boldsymbol{r}^T\boldsymbol{I}\dot{\boldsymbol{r}} + \boldsymbol{\Xi}^T\boldsymbol{K}_s\dot{\boldsymbol{\Xi}} + \left(\int \boldsymbol{T}^T\boldsymbol{\Xi}\, d\tau\right)^T \boldsymbol{B}\boldsymbol{\Lambda}\boldsymbol{K}_s\boldsymbol{T}^T\boldsymbol{\Xi} \\
&= -\boldsymbol{r}^T\boldsymbol{K}\boldsymbol{r} - \boldsymbol{r}^T\boldsymbol{K}_s\boldsymbol{T}^T\boldsymbol{\Xi} + \boldsymbol{\Xi}^T\boldsymbol{K}_s\dot{\boldsymbol{\Xi}} \\
&\quad + \left(\int \boldsymbol{T}^T\boldsymbol{\Xi}\, d\tau\right)^T \boldsymbol{B}\boldsymbol{\Lambda}\boldsymbol{K}_s\boldsymbol{T}^T\boldsymbol{\Xi}
\end{aligned} \tag{35}
$$

Replacing $\boldsymbol{r}$ in the second term of (35) with (21, 22, 26),

$$
\begin{aligned}
\dot{V}(\boldsymbol{r}, \boldsymbol{\Xi}) &= -\boldsymbol{r}^T\boldsymbol{K}\boldsymbol{r} - \left[\dot{\boldsymbol{E}} + \boldsymbol{B}\boldsymbol{T}^T\boldsymbol{\Xi} + \boldsymbol{\Lambda}\boldsymbol{E} + \boldsymbol{B}\boldsymbol{\Lambda}\boldsymbol{T}^T\int \boldsymbol{\Xi}\, d\tau\right]^T \\
&\quad \times \boldsymbol{K}_s\boldsymbol{T}^T\boldsymbol{\Xi} + \boldsymbol{\Xi}^T\boldsymbol{K}_s\dot{\boldsymbol{\Xi}} + \left(\int \boldsymbol{T}^T\boldsymbol{\Xi}\, d\tau\right)^T \boldsymbol{B}\boldsymbol{\Lambda}\boldsymbol{K}_s\boldsymbol{T}^T\boldsymbol{\Xi} \\
&= -\boldsymbol{r}^T\boldsymbol{K}\boldsymbol{r} - [\dot{\boldsymbol{E}} + \boldsymbol{B}\boldsymbol{T}^T\boldsymbol{\Xi} + \boldsymbol{\Lambda}\boldsymbol{E}]^T\boldsymbol{K}_s\boldsymbol{T}^T\boldsymbol{\Xi} + \boldsymbol{\Xi}^T\boldsymbol{K}_s\dot{\boldsymbol{\Xi}} \\
&= -\boldsymbol{r}^T\boldsymbol{K}\boldsymbol{r} - \dot{\boldsymbol{E}}^T\boldsymbol{K}_s\boldsymbol{T}^T\boldsymbol{\Xi} - \boldsymbol{\Xi}^T\boldsymbol{T}\boldsymbol{B}\boldsymbol{K}_s\boldsymbol{T}^T\boldsymbol{\Xi} \\
&\quad - \boldsymbol{E}^T\boldsymbol{\Lambda}\boldsymbol{K}_s\boldsymbol{T}^T\boldsymbol{\Xi} + \boldsymbol{\Xi}^T\boldsymbol{K}_s\dot{\boldsymbol{\Xi}} \\
&= -\boldsymbol{r}^T\boldsymbol{K}\boldsymbol{r} - (\boldsymbol{T}\dot{\boldsymbol{E}})^T\boldsymbol{K}_s\boldsymbol{\Xi} - \boldsymbol{\Xi}^T\boldsymbol{T}\boldsymbol{B}\boldsymbol{K}_s\boldsymbol{T}^T\boldsymbol{\Xi} \\
&\quad - (\boldsymbol{T}\boldsymbol{E})^T\boldsymbol{\Lambda}\boldsymbol{K}_s\boldsymbol{\Xi} + \boldsymbol{\Xi}^T\boldsymbol{K}_s\dot{\boldsymbol{\Xi}} \\
&= -\boldsymbol{r}^T\boldsymbol{K}\boldsymbol{r} - (\boldsymbol{T}^T\boldsymbol{\Xi})^T\boldsymbol{B}\boldsymbol{K}_s\boldsymbol{T}^T\boldsymbol{\Xi} - \boldsymbol{\Xi}^T\boldsymbol{\Lambda}\boldsymbol{K}_s\boldsymbol{\Xi}
\end{aligned}
$$

Because $\boldsymbol{K}$, $\boldsymbol{B}\boldsymbol{K}_s$, and $\boldsymbol{\Lambda}\boldsymbol{K}_s$ are all positive-definite matrices, we conclude that

$$
\dot{V}(\boldsymbol{r}, \boldsymbol{\Xi}) = -\boldsymbol{r}^T\boldsymbol{K}\boldsymbol{r} - (\boldsymbol{T}^T\boldsymbol{\Xi})^T\boldsymbol{B}\boldsymbol{K}_s\boldsymbol{T}^T\boldsymbol{\Xi} - \boldsymbol{\Xi}^T\boldsymbol{\Lambda}\boldsymbol{K}_s\boldsymbol{\Xi} \leq 0 \tag{36}
$$

Since $\dot{V}(\boldsymbol{r}, \boldsymbol{\Xi}) \leq 0$ in (36), the $V(\boldsymbol{r}, \boldsymbol{\Xi})$ given in (31) is either decreasing or constant. Due to the fact that $V(\boldsymbol{r}, \boldsymbol{\Xi})$ is nonnegative we conclude that $V(\boldsymbol{r}, \boldsymbol{\Xi}) \in \mathcal{L}_\infty$; hence $\boldsymbol{r} \in \mathcal{L}_\infty$. With $\boldsymbol{r} \in \mathcal{L}_\infty$ we conclude from (26) that $\dot{\boldsymbol{E}}^*(t) \in \mathcal{L}_\infty$ and $\boldsymbol{E}^*(t) \in \mathcal{L}_\infty$, and $\boldsymbol{E}(t), \dot{\boldsymbol{E}}(t), \boldsymbol{\Xi}(t), \dot{\boldsymbol{\Xi}}(t) \in \mathcal{L}_\infty$ based on their definitions. Because of the boundedness of $\boldsymbol{\Theta}_d(t)$ and $\dot{\boldsymbol{\Theta}}_d(t)$ we conclude that $\boldsymbol{\Theta}(t) \in \mathcal{L}_\infty$ and $\dot{\boldsymbol{\Theta}}(t) \in \mathcal{L}_\infty$ from (14). With the previous boundedness statements and the fact that $\ddot{\boldsymbol{\Theta}}_d(t)$ is also bounded, $\boldsymbol{\Phi} \in \mathcal{L}_\infty$ and $\tilde{\boldsymbol{N}}(\cdot) \in \mathcal{L}_\infty$ can be concluded from their definitions. Hence, the control input $\boldsymbol{V}(t) \in \mathcal{L}_\infty$ is also determined from (29). The preceding information can also be used to (9) and (33) to get $\ddot{\boldsymbol{\Theta}}(t)$, $\dot{\boldsymbol{r}}(t) \in \mathcal{L}_\infty$. Now we have explicitly illustrated that all signals in the synchronisation trajectory tracking controller and system remain bounded during the closed-loop operation.

From (36) we show that $\boldsymbol{r}(t) \in \mathcal{L}_2, \boldsymbol{T}^T\boldsymbol{\Xi}(t) \in \mathcal{L}_2$ and $\boldsymbol{\Xi}(t) \in \mathcal{L}_2$. Hence, $\lim_{t\to\infty} \boldsymbol{r}(t) = 0$ and $\lim_{t\to\infty} \boldsymbol{\Xi}(t) = 0$ can be obtained according to corollary 1.1 in [15]. Furthermore, we conclude that $\lim_{t\to\infty} \boldsymbol{E}^*(t), \dot{\boldsymbol{E}}^*(t) = 0$ using lemma 1.6 in [15].

When $\boldsymbol{\Xi}(t) = 0$, i.e. $\varepsilon_i(t) = 0$ for $i = 1, 2, \ldots, n$, we know from the synchronisation errors in (18, 19) that

$$
\boldsymbol{e}_1(t) = \boldsymbol{e}_2(t) = \cdots = \boldsymbol{e}_n(t) \tag{37}
$$

Also, from the coupled attitude errors in (23, 24) we get

$$
\boldsymbol{e}_1^*(t) + \boldsymbol{e}_2^*(t) + \cdots + \boldsymbol{e}_n^*(t) = \boldsymbol{e}_1(t) + \boldsymbol{e}_2(t) + \cdots + \boldsymbol{e}_n(t) \tag{38}
$$

Because of $\lim_{t\to\infty} \boldsymbol{E}^*(t) = 0$ we conclude that

$$
\boldsymbol{e}_1(t) = \boldsymbol{e}_2(t) = \cdots = \boldsymbol{e}_n(t) = 0 \tag{39}
$$

From (36) and the foregoing derivation we know that $\dot{V}(\cdot) = 0$ only if $\boldsymbol{E}(t) = 0$. Using LaSalle's theorem [16], $\lim_{t\to\infty} \boldsymbol{E}(t) = 0$ can be concluded. Thus we finally reach

$$
\lim_{t\to\infty} \boldsymbol{E}(t), \boldsymbol{\Xi}(t) = 0
$$

□

4 Experiments

The experiments are conducted on the multiple 3-DOF helicopter setup, which includes three 3-DOF helicopters as shown in Fig. 4. The parameters for these three 3-DOF helicopters are given in Table 1.

As an initial-stage experimental investigation we applied the proposed synchronisation controller to only one axis of the laboratory helicopters, i.e. the elevation axis, and keep the controllers for other axes (pitch and travel) unchanged, using the Quanser-provided LQR controller. By checking the dynamic equation in (6) we learn that the elevation motion and pitch motion are uncoupled. The elevation motion does not influence the pitch motion and the elevation motion is stable if the pitch motion is stable. Moreover, the controller structure illustrated in Fig. 3 shows that the synchronisation process is operated among the same axis (attitude motion), but not among different axes. Thus it is reasonable to apply the proposed synchronisation controller to one DOF only and different controllers to other DOFs and still guarantee the stability of the whole system. Note that the proposed synchronisation controller can be applied to the multiple degrees-of-freedom experiment.

A quintic polynomial trajectory in (40) is designed for the attitude motion of the elevation.

$$
\begin{aligned}
\alpha_d(t) &= C_0 + C_1 t + C_2 t^2 + C_3 t^3 + C_4 t^4 + C_5 t^5 = \sum_{i=0}^{5} C_i t^i \\
\dot{\alpha}_d(t) &= C_1 + 2C_2 t + 3C_3 t^2 + 4C_4 t^3 + 5C_5 t^4 = \sum_{i=1}^{5} i C_i t^{i-1} \\
\ddot{\alpha}_d(t) &= 2C_2 + 6C_3 t + 12C_4 t^2 + 20C_5 t^3 = \sum_{i=2}^{5} i(i-1) C_i t^{i-2}
\end{aligned} \tag{40}
$$

where the coefficients $C_0 \sim C_5$ can be determined from the position, velocity and acceleration requirements at both boundaries. If the desired maneuvre is from 0 to 30 deg in 8 s, the coefficients are $C_0 = C_1 = C_2 = 0$, $C_3 = 0.5859$, $C_4 = -0.1099$ and $C_5 = 0.0055$. The trajectory guarantees that $\alpha(t) \in \mathcal{L}_\infty, \dot{\alpha}(t) \in \mathcal{L}_\infty$, and $\ddot{\alpha}(t) \in \mathcal{L}_\infty$.

The control gains are tuned by trial and error until a good trajectory tracking performance is achieved, and the final values used in our experiments are also given in Table 1.

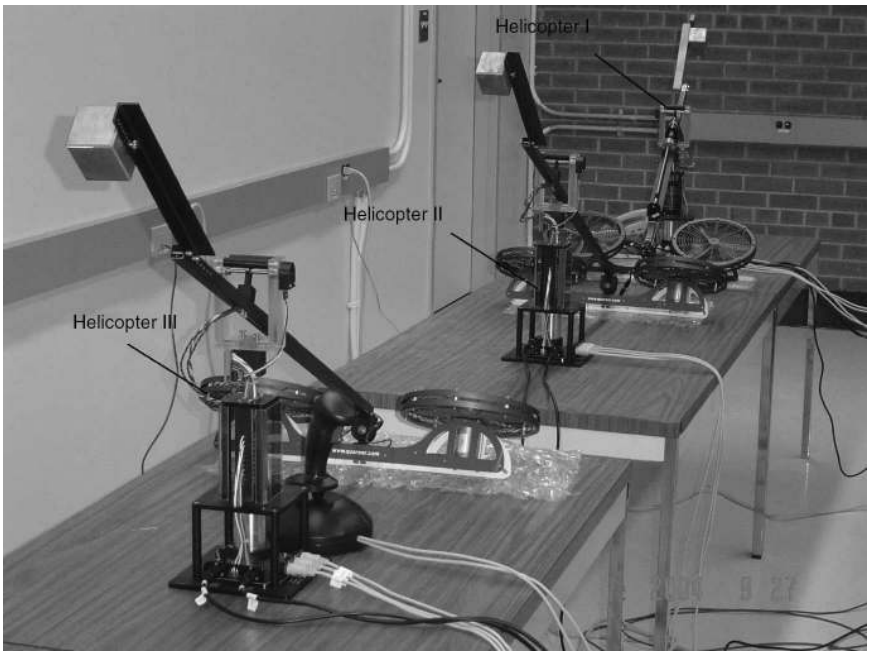

Fig. 4 *Three 3-DOF helicopters experimental setup*

Table 1: Parameters and control gains for three 3-DOF helicopters

Parameters/gains	Helicopter I	Helicopter II	Helicopter III
Moment of inertia J_{ei}, kg · m^2	1.044	1.030	1.017
Moment of inertia J_{pi}, kg · m^2	0.0455	0.0455	0.0455
Mass m_i, kg	0.142*	0.128	0.113
K_{fi}, N/V	0.625	0.625	0.625
l_{ai}, m	0.648	0.648	0.648
l_{hi}, m	0.178	0.178	0.178
ADS system	yes	no	no
Feedback gains for elevation, $[K_P, K_D]$	[30.0 15.0]	[30.0 15.0]	[30.0 15.0]
Sync. feedback gains, K_{si}	1.0	1.0	1.0
Sync. coupling gains, B_i	1.0	1.0	1.0

*Value measured when ADS is at farthest position from propellers, 0.170 for middle position in slide bar, 0.213 for nearest position from propellers.

For comparison between different synchronisation errors, two synchronisation strategies are considered: *Strategy I*: The synchronisation error and the coupled attitude error are chosen to be those in (18) and (23); *Strategy II*: The synchronisation error and the coupled attitude error are those in (19) and (24). The synchronisation error in (18) is employed as the uniform synchronisation error for performance evaluation in all experiments. Furthermore, the ADS on Helicopter I is activated by a square wave command, see Fig. 5, for performing disturbance to the control system. In this way the effective mass of Helicopter I will vary between 0.142 and 0.213 kg. The asymptotic convergences of both trajectory tracking and synchronisation errors can only be realised when the exact system parameters are known. If there is a parametric disturbance, such as the mass disturbance in our case, the asymptotic convergence cannot be guaranteed although the system may still be stable. The aim of introducing the mass disturbance in our experiments is to verify the effectiveness of the proposed controller. We

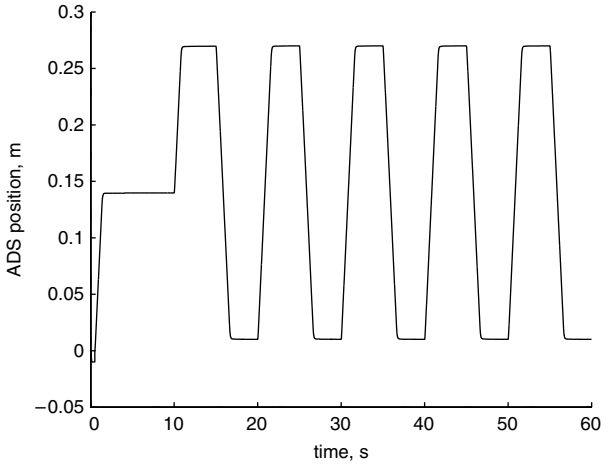

Fig. 5 *ADS position trajectory*
0 means ADS is at farthest position from propellers, 0.26 means ADS is at nearest position from propellers

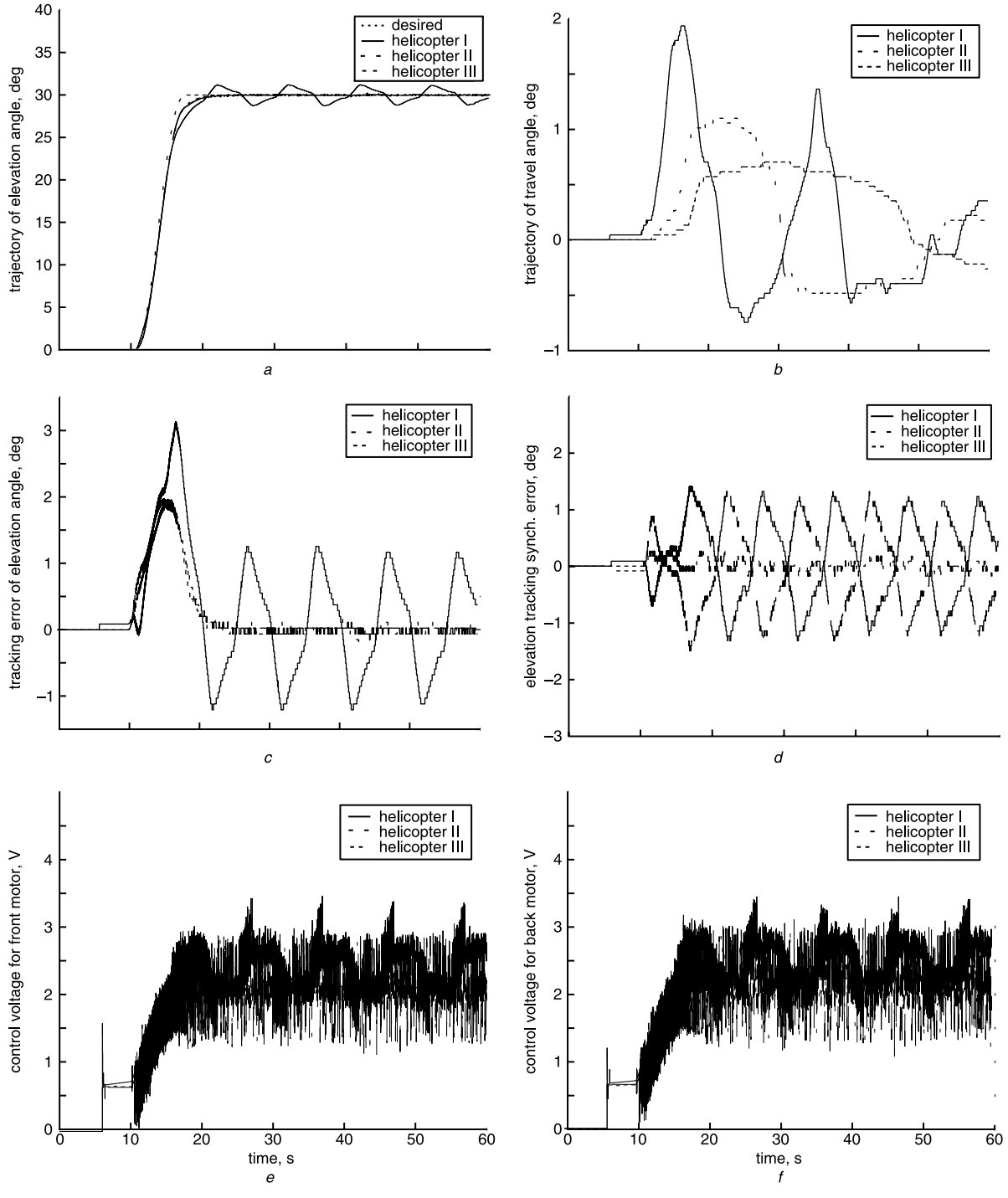

Fig. 6 *Experimental result of attitude trajectory tracking control without synchronisation strategy*

a Trajectories of elevation angle
b Trajectories of travel angle
c Trajectory tracking errors of elevation angle
d Synchronisation errors of elevation angle
e Control voltages for front motors
f Control voltages for back motors

inspect how these 3-DOF helicopters response without /with synchronisation strategies, and compare the synchronisation performance using different synchronization strategies under the parametric disturbance.

Figure 6 shows the experimental results of elevation tracking control of three 3-DOF helicopters without synchronisation strategy (by setting $K_{si} = 0$ and $B_i = 0$). Figures 7 and 8 are the experimental results using synchronisation strategy I and II, respectively. The maximal elevation tracking and synchronisation errors are measured and listed in Table 2. For each experiment the three values present the maximal elevation trajectory tracking errors during maneuver (from 0 to 20 s), after maneuver (maneuver completed, after 20 s in our experiments), and the maximal synchronisation error during whole experiment, respectively.

It can be seen from Fig. 6 that the elevation trajectory tracking error of Helicopter I is large because of the ADS. Table 2 shows that the maximal elevation trajectory tracking errors during and after the maneuver are 3.136

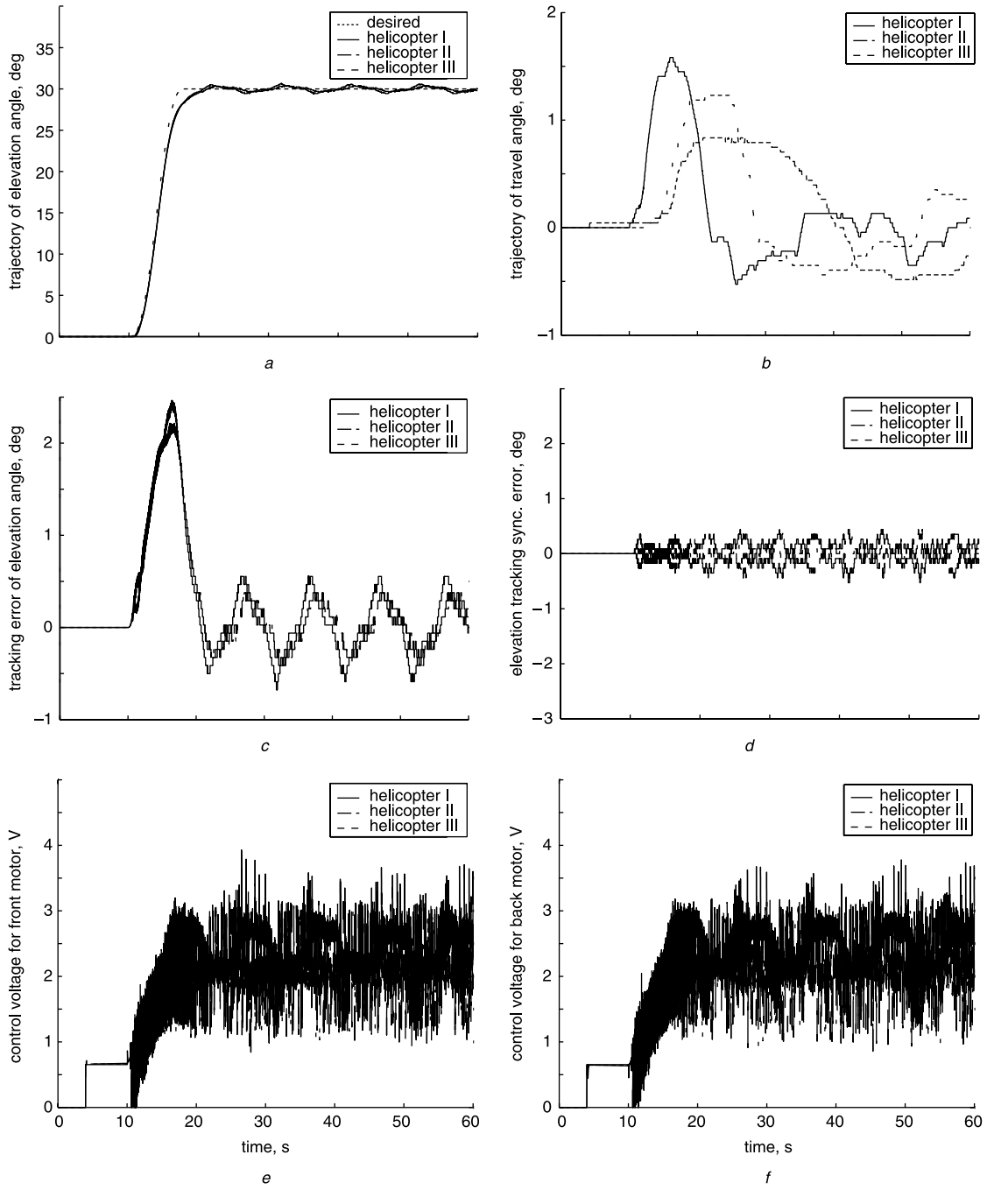

Fig. 7 *Experimental result of attitude trajectory tracking control with synchronisation strategy I*

a Trajectories of elevation angle
b Trajectories of travel angle
c Trajectory tracking errors of elevation angle
d Synchronisation errors of elevation angle
e Control voltages for front motors
f Control voltages for back motors

and 1.257 deg, respectively. As there is no interconnection between these 3-DOF helicopters, the elevation tracking motion of Helicopter II and III do not react to the tracking motion of Helicopter I due to ADS. Thus, the asymptotic convergences of Helicopter II and III have been achieved. For this reason the synchronisation errors between them are large and the maximal value is 1.319 deg. However, the elevation trajectory tracking and synchronisation errors can be reduced remarkably by using the proposed synchronisation strategies. For example, the maximal synchronisation error has been reduced to 0.527 deg using strategy I and further to 0.506 deg using strategy II.

As discussed previously, synchronisation strategy II is expected to produce better performance than strategy I because it employs more adjoining helicopters' information in each individual controller. However, this better performance is obtained at the cost of more online computation burden, less reliability, and more control efforts, which can be seen by comparing the experimental figures of control voltages for all cases. Videos of these experiments can be found at http://arrow.utias.utoronto.ca/~liu/.

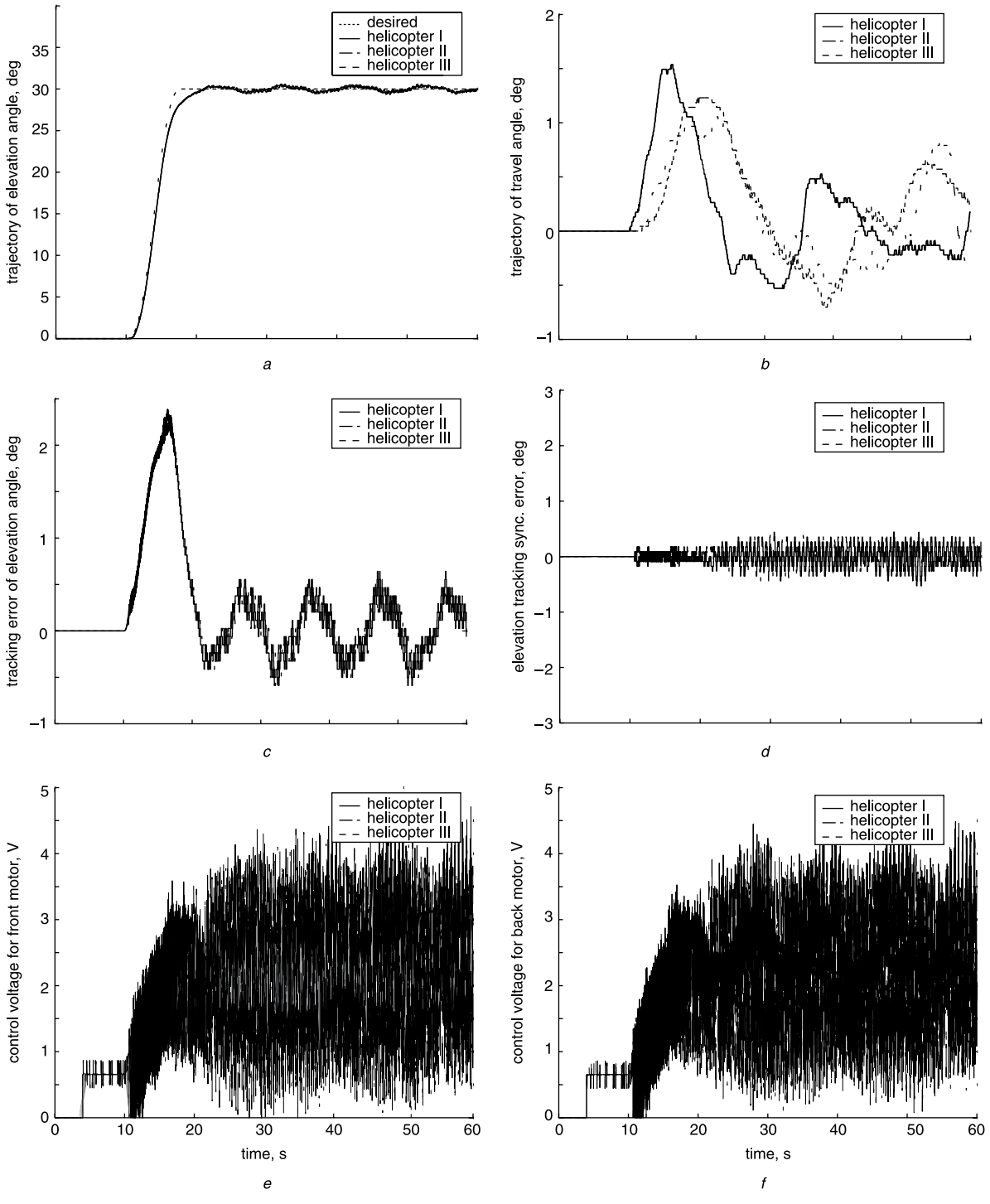

Fig. 8 *Experimental result of attitude trajectory tracking control with synchronisation strategy II*

a Trajectories of elevation angle
b Trajectories of travel angle
c Trajectory tracking errors of elevation angle
d Synchronisation errors of elevation angle
e Control voltages for front motors
f Control voltages for back motors

5 Conclusions

This paper has presented a model-based synchronised trajectory tracking control strategy for multiple three-degrees-of-freedom (3-DOF) helicopters. With the proposed synchronisation controller, both the attitude trajectory tracking errors and the attitude synchronisation errors can achieve asymptotic convergence. The introduction of the generalised synchronisation concept allows more space for designing different synchronisation errors.

Experimental results conducted on the three 3-DOF helicopters setup verify the effectiveness of the proposed synchronisation controller. The investigation indicates that better performance can be realised at the cost of computational burden, reliability, and control efforts. A tradeoff between the synchronisation performance and the

Table 2: Maximal elevation tracking errors and synchronisation errors (deg)

Strategy	Helicopter I	Helicopter II	Helicopter III
No	3.136	1.968	1.978
	1.257	0.290	0.378
	1.319	0.264	1.319
I	2.466	2.217	2.206
	0.677	0.466	0.466
	0.527	0.264	0.440
II	2.385	2.261	2.259
	0.641	0.641	0.641
	0.506	0.440	0.352

implementation costs should be made before applying the suitable synchronisation strategy to the real system.

Future work under investigation includes: an adaptive synchronisation controller for system with parametric variation; and development of a new synchronisation strategy.

6 References

1 Blekhman, I.I., Landa, P.S., and Rosenblum, M.G.: 'Synchronization and chaotization in interacting dynamical systems', *ASME Appl. Mech. Rev.*, 1995, **48**, (11), pp. 733–752

2 Rodriguez-Angeles, A., and Nijmeijer, H.: 'Mutual synchronization of robots via estimated state feedback: a cooperative approach', *IEEE Trans. Control Syst. Technol.*, 2004, **12**, (4), pp. 542–554

3 Nijmeijer, H., and Rodriguez-Angeles, A.: 'Synchronization of mechanical systems' (World Scientific, Singapore, 2003)

4 Koren, Y.: 'Cross-coupled biaxial computer controls for manufacturing systems', *J. Dyn. Syst., Meas., Control*, 1980, **102**, (2), pp. 256–272

5 Tomizuka, M., Hu, J.S., Chiu, T.C., and Kamano, T.: 'Synchronization of two motion control axes under adaptive feedforward control', *J. Dyn. Syst., Meas., Control*, 1992, **114**, (6), pp. 196–203

6 Yang, L.F., and Chang, W.H.: 'Synchronization of twin-gyro precession under cross-coupled adaptive feedforward control', *J. Guid. Control, Dynam.*, 1996, **19**, (3), pp. 534–539

7 Wang, P.K.C., Yee, J., and Hadaegh, F.Y.: 'Synchronized rotation of multiple autonomous spacecraft with rule-based controls: experimental study', *J. Guid. Control, Dynam.*, 2001, **24**, (2), pp. 352–359

8 Levine, J.: 'On the synchronization of a pair of independent windshield wipers', *IEEE Trans. Control Syst. Technol.*, 2004, **12**, (5), pp. 787–795

9 Aguiar, A.P., Cremean, L., and Hespanha, J.P.: 'Position tracking for a nonlinear underactuated hovercraft: Controller design and experimental results'. Proc. of IEEE Conf. on Decision and Control, December 2002, pp. 3858–3863

10 Wu, X.F., Liu, Y., and Zhu, J.J.: 'Design and real time testing of a trajectory linearization flight controller for the Quanser UFO'. Proc. of American Control Conf., June 2003, pp. 3913–3918

11 Castillo, P., Dzul, A., and Lozano, R.: 'Real-time stabilization and tracking of a four-rotor mini rotorcraft', *IEEE Trans. Control Syst. Technol.*, 2004, **12**, (4), pp. 510–516

12 Vladimerou, V., Stubbs, A., Rubel, J., Fulford, A., and Dullerud, G.: 'A hovercraft testbed for decentralized and cooperative control'. Proc. of American Control Conf., June 2004, pp. 5332–5337

13 Kutay, A.T., Calise, A.J., Idan, M., and Hovakimyan, N.: 'Experimental results on adaptive output feedback control using a laboratory model helicopter', *IEEE Trans. Control Syst. Technol.*, 2005, **13**, (2), pp. 196–202

14 Sun, D.: 'Position synchronization of multiple motion axes with adaptive coupling control', *Automatica*, 2003, **39**, (6), pp. 997–1005

15 Dawson, D.M., Hu, J., and Burg, T.C.: 'Nonlinear control of electric machinery' (Marcel Dekker, New York, 1998)

16 Khalil, H.: 'Nonlinear systems' (Prentice Hall, Englewood Cliffs, NJ, 1996)